Subduction factory: 4. Depth-dependent flux of H_2O from subducting slabs worldwide

Peter E. van Keken,[1] Bradley R. Hacker,[2] Ellen M. Syracuse,[3] and Geoff A. Abers[4]

Received 9 August 2010; revised 19 October 2010; accepted 26 October 2010; published 5 January 2011.

[1] A recent global compilation of the thermal structure of subduction zones is used to predict the metamorphic facies and H_2O content of downgoing slabs. Our calculations indicate that mineralogically bound water can pass efficiently through old and fast subduction zones (e.g., in the western Pacific), whereas hot subduction zones such as Cascadia see nearly complete dehydration of the subducting slab. The top of the slab is sufficiently hot in all subduction zones that the upper crust, including sediments and volcanic rocks, is predicted to dehydrate significantly. The degree and depth of dehydration in the deeper crust and uppermost mantle are highly diverse and depend strongly on composition (gabbro versus peridotite) and local pressure and temperature conditions. The upper mantle dehydrates at intermediate depths in all but the coldest subduction zones. On average, about one third of the bound H_2O subducted globally in slabs reaches 240 km depth, carried principally and roughly equally in the gabbro and peridotite sections. The predicted global flux of H_2O to the deep mantle is smaller than previous estimates but still amounts to about one ocean mass over the age of the Earth. At this rate, the overall mantle H_2O content increases by 0.037 wt % (370 ppm) over the age of the Earth. This is qualitatively consistent with inferred H_2O concentrations in the Earth's mantle assuming that secular cooling of the Earth has increased the efficiency of volatile recycling over time.

Citation: van Keken, P. E., B. R. Hacker, E. M. Syracuse, and G. A. Abers (2011), Subduction factory: 4. Depth-dependent flux of H_2O from subducting slabs worldwide, *J. Geophys. Res.*, *116*, B01401, doi:10.1029/2010JB007922.

1. Introduction

[2] Large amounts of water enter the world's subduction zones at a trench. At shallow depths compaction causes fluids to be expelled, but a significant amount remains mineralogically bound in the sediments, crust, and potentially the uppermost mantle of the downgoing slab. When the slab comes in contact with the hot mantle wedge, a series of dehydration reactions (that depend on composition, pressure p, and temperature T) take place. This provides the main source for fluids that cause flux melting in the mantle wedge [e.g., *Grove et al.*, 2006], which in turn causes the formation of volcanoes and the growth of arc crust.

[3] Important questions remain regarding the mechanism and location of fluid release from subducting slabs and the amount of water that can be retained in the slab and subsequently can be recycled to the deep mantle. While improved analyses of fluid and gas inclusions have made inferences of volatile contents in the arc source more robust [e.g., *Wallace*, 2005; *Shaw et al.*, 2008; *Kelley et al.*, 2010], it remains difficult to provide precise global mass balance computations of volatile cycling in subduction zones due to incomplete sampling. The most recent global estimates generally provide extrapolations from the more robust observations of CO_2 and SO_2 outgassing [e.g., *Hilton et al.*, 2002; *Wallace*, 2005]. *Wallace* [2005] provides an estimate of a global flux of 3×10^8 Tg/Myr outgassing of H_2O and suggests that there is an approximate balance between the input of structurally bound H_2O and that returned in arcs. This suggests that slabs are completely dehydrated and that minimal H_2O is returned to the deeper mantle. It is important to constrain the flux of water to the deeper Earth, because even small amounts of water have significant effects on viscosity [e.g., *Hirth and Kohlstedt*, 1996; *Jung and Karato*, 2001] and melt productivity [*Hirschmann*, 2006], thereby directly influencing mantle convection, plate tectonics, and chemical differentiation, and ultimately the long-term chemical and thermal evolution of the Earth.

[4] Seismic array studies have made it possible to illuminate the mantle wedge and subducting slab. The reduction in seismic velocities and quality factor Q make it possible to image regions of hydrated crust and mantle [*Rondenay et al.*, 2008; *Nakajima et al.*, 2009] and demonstrate the likely pathways of fluids and melt [*Syracuse et al.*, 2008;

[1]Department of Geological Sciences, University of Michigan, Ann Arbor, Michigan, USA.
[2]Department of Earth Science, University of California, Santa Barbara, California, USA.
[3]Department of Geoscience, University of Wisconsin–Madison, Madison, Wisconsin, USA.
[4]Lamont-Doherty Earth Observatory, Columbia University, Palisades, New York, USA.

0148-0227/11/2010JB007922

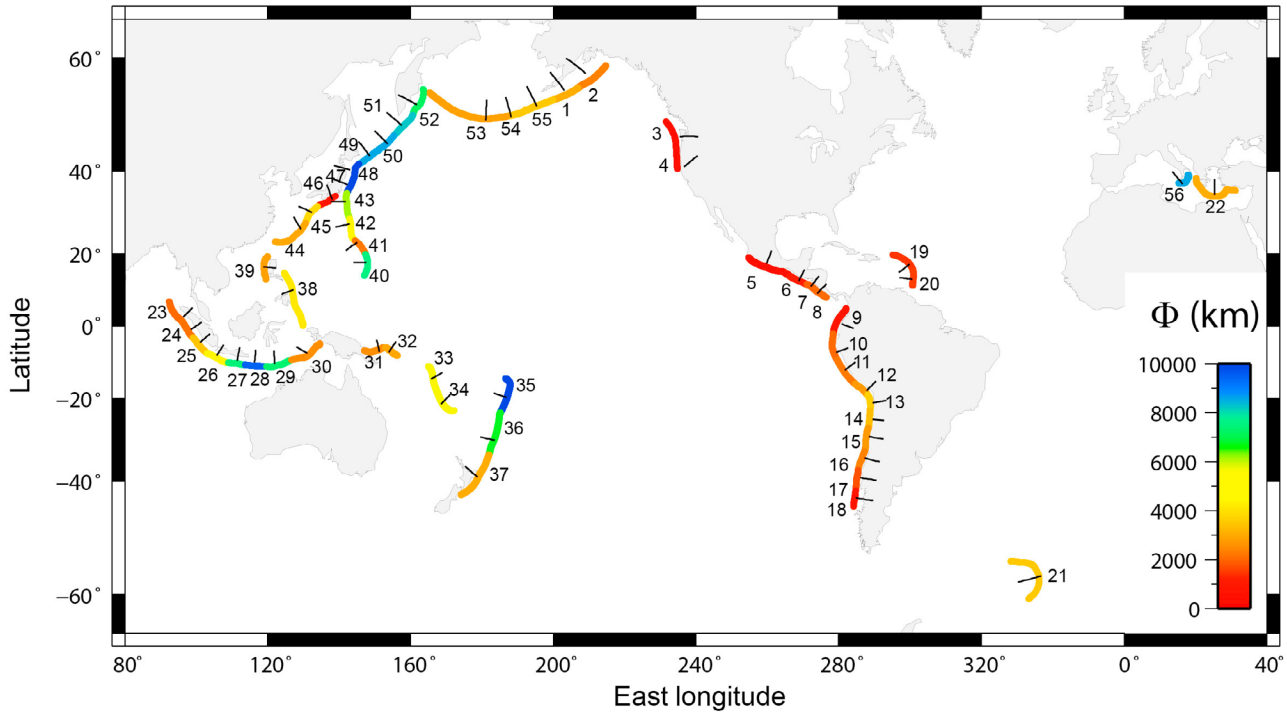

Figure 1. Location map of the 2-D subduction zone models used in this study. The trench is colored with thermal parameter Φ defined as the product of convergence speed and age (km). Black lines indicate the location and azimuth of the 2-D cross sections. Numbers indicate the subduction zone (1, Alaska Peninsula; 2, Alaska; 3, British Columbia; 4, Cascadia; 5, Mexico; 6, Guatemala-El Salvador; 7, Nicaragua; 8, Costa Rica; 9, Columbia-Ecuador; 10, North Peru; 11, Central Peru; 12, Peru; 13, North Chile; 14, North Central Chile; 15, Central Chile A; 16, Central Chile B; 17, South Central Chile; 18, South Chile; 19, Northern Lesser Antilles; 20, Southern Lesser Antilles; 21, Scotia; 22, Aegean; 23, North Sumatra; 24, Central Sumatra; 25, South Sumatra; 26, Sunda Strait; 27, Java; 28, Bali-Lombok; 29, West Banda Sea; 30, East Banda Sea; 31, New Britain; 32, Solomon; 33, North Vanuatu; 34, South Vanuatu; 35, Tonga; 36, Kermadec; 37, New Zealand; 38, Southern Philippines; 39, Northern Philippines; 40, South Marianas; 41, North Marianas; 42, Bonin; 43, Izu; 44, Kyushu; 45, Ryukyu; 46, Nankai; 47, Central Honshu; 48, Tohoku; 49, Hokkaido; 50, Southern Kuriles; 51, Northern Kuriles; 52, Kamchatka; 53, Western Aleutians; 54, Central Aleutians; 55, Eastern Aleutians; 56, Calabria).

Rychert et al., 2008], although effects of water on seismic observables remain incompletely calibrated [*Aizawa et al.*, 2008]. Intermediate-depth seismicity in the crust and upper mantle has been linked to dehydration reactions [e.g., *Kirby et al.*, 1996]. High-resolution images of the position of earthquakes in the slab provide intriguing support for this by demonstrating the similarity in position of intermediate-depth seismicity with the predicted location of the main dehydration reactions [*Abers et al.*, 2006; *Kita et al.*, 2006]. In order to quantitatively relate these observations to dehydration reactions, it is essential to develop petrological models that predict the location of the main dehydration reactions in specific subduction zones.

[5] We present here a compilation of 56 subduction zone segments for which we predict temperature, mineral stabilities, and water content. The thermal models are based on those presented by *Syracuse et al.* [2010]. The petrological modeling is similar to that given by *Hacker* [2008] but incorporates significant improvements by using (1) an updated thermodynamic description (with the inclusion of melting) and (2) high-resolution finite element models for each subduction zone, which allows for a high-resolution determination of the metamorphic facies in the subduction slab. We use this global compilation to estimate the total flux of water into the mantle wedge and the deeper mantle. This paper is the fourth in a series discussing thermal, petrological, and seismological constraints on the "subduction factory" [*Hacker et al.*, 2003a, 2003b; *Hacker and Abers*, 2004].

2. Methods

2.1. Finite Element Models for Subduction Zone Thermal Structure

[6] We use the subduction zone models described by *Syracuse et al.* [2010]. The subduction zone models cover the world's major trenches in 56 segments and are based on 2-D cross sections normal to the trench (Figure 1). The locations of the segments are based on the global geometry compilation of *Syracuse and Abers* [2006] and have an average spacing of approximately 700 km. The geometry of each slab is based on an along-trench average for the segment. The temperature in the slab is predicted using a kinematic-dynamic approach similar to that of *Peacock and Wang* [1999] and *van Keken et al.* [2002] wherein the

Table 1. Sediment Types Used in Modeling

Rock Type	ODP Site	SiO_2	TiO_2	Al_2O_3	FeO	MnO	MgO	CaO	Na_2O	K_2O	H_2O
carbonate	Guatemala site 495	13.3	0.0	0.7	3.7		1.3	44.5	0.4	0.3	0.5
chert	Mariana site 800	88.7	0.1	2.3	1.3	0.3	0.7	0.4	0.5	0.6	0.8
terrigenous	Antilles "pc"	55.2	0.9	20.8	6.0	0.1	2.2	0.5	0.6	3.0	5.2
diatomaceous ooze	Kurile Site 579	70.8	0.5	12.2	4.9		2.2	0.7	3.5	2.3	2.3
pelagic	Mariana site 800	49.8	0.6	14.7	7.3	2.1	3.1	3.5	3.1	3.6	6.5
turbidite	Alaska Site 178	57.9	0.8	15.4	6.0		3.0	2.4	2.9	2.4	9.2

velocity in the slab is prescribed but the flow in the wedge is dynamically generated. The speed of the slab is given by the trench-normal component of the convergence velocity and is assumed to remain parallel to the slab surface. We base the wedge viscosity on the dry olivine flow laws of *Karato and Wu* [1993]. We ignore thermal buoyancy in the wedge. The principal driving force for wedge convection is the coupling to the downgoing slab. We use the "D80" models of *Syracuse et al.* [2010], in which the slab is fully decoupled from the overriding plate along the seismogenic zone (assumed to end at 40 km), partially coupled to a depth of 80 km, and fully coupled below this depth. The partial decoupling below the seismogenic zone is necessary to generate the "cold nose" of the wedge that is inferred for many subduction zones based on observations of seismic properties and heat flow [e.g., *Furukawa and Uyeda*, 1989; *Hashida*, 1989; *Hyndman and Peacock*, 2003; *Stachnik et al.*, 2004; *Yoshimoto et al.*, 2006; *Rychert et al.*, 2008] and has been suggested to be a global phenomenon [*Wada and Wang*, 2009].

[7] The governing equations are solved on a high-resolution finite element mesh (with 1 km resolution in the wedge tip and thermal boundary layers) using the finite element package Sepran [*Cuvelier et al.*, 1986]. The subduction zone thermal models were benchmarked with several independent codes by *van Keken et al.* [2008]. With a few exceptions [see *Syracuse et al.*, 2010] we model the evolution of each subduction zone for 20 Myr, which is sufficient to reach a quasi steady state thermal structure. For a full description of the model assumptions, equations, and solution techniques, see *Syracuse et al.* [2010].

[8] To expand the results for a single cross section to the corresponding subduction zone segment, we assign a length to each segment. This length is determined as follows. For trenches that are represented by a single subduction zone, we use the trench length measured from the maps by *Syracuse and Abers* [2006]. For segments with multiple subduction zones (e.g., Alaska-Aleutians, Tonga-Kermadec-New Zealand), we determine the length of the representative segment by the location of the cross section. For strongly arcuate trenches (Marianas, Scotia, Calabria) we estimate the effective trench length perpendicular to the convergence velocity. In Calabria and Scotia we exclude the segments that are subparallel to the convergence vector. We have excluded a few trenches for which we do not have representative models (e.g., Makran, Yap-Palau). The total effective length is approximately 38,500 km, which is more than 90% of the combined trench length reported by *Clift and Vannucchi* [2004] and *Scholl and von Huene* [2007]. The locations and assumed trench lengths are reported in Table 2.

2.2. Petrological Modeling

[9] According to *Hacker* [2008], the slab crust consists of a sediment layer of variable thickness and composition, a 300 m thick upper volcanic layer, a 300 m thick lower volcanic layer, 1.4 km of dikes, and 5 km of gabbro. We assume that at input the pore fluids have been expelled and that all water is chemically bound in hydrous phases. The input composition is based on the phases at 15 km depth and at the temperature predicted by the thermal models. The amount of sediment being subducted at each trench is based on the compilations of *Clift and Vannucchi* [2004] and *Scholl and von Huene* [2007] and includes the effects of compaction and the off scraping of sediments into the accretionary prism. The composition of the subducted sediment in each cross section was assigned one of six types (based on the methods of *Plank and Langmuir* [1998]), which are the four used by *Hacker* [2008] plus a diatomaceous ooze and a turbidite (Table 1). The bulk compositions for the upper volcanic layer, the lower volcanic layer, and dikes were chosen to be mid-ocean ridge basalt (MORB), with the slab-age-dependent K_2O and H_2O contents given by *Jarrard* [2003].

[10] The extent to which the upper mantle below the crust is hydrated is poorly known. *Hacker* [2008] summarized the uncertainties regarding hydration of the slab mantle, concluding that a limit of 2 wt % H_2O in the upper 4 km of the mantle is a reasonable global average. Here we use three different assumptions for the hydration state of the upper 2 km: dry, 2 wt % H_2O, and fully saturated. We will use the moderate hydration case as base model but will provide a discussion of the consequences of assumptions of zero or full hydration. As demonstrated earlier [e.g., *Schmidt and Poli*, 2003], the slab mantle may carry the bulk of the slab H_2O to profound depths. Obtaining better constraints on slab-mantle hydration should be a priority.

[11] In the modeling we ignore the contribution of continental crust subduction and erosion, because the overall contribution to the water budget is modest (~16% [*Hacker*, 2008]) and we can add this as an a posteriori correction. Phase relations in the slab and overlying mantle wedge were calculated at subsolidus conditions following the methodology of *Hacker* [2008], using Perple_X version 7 [*Connolly*, 2009] and the 2004 version of the *Holland and Powell* [1998] thermodynamic database. The phase relations were calculated for H_2O saturation. We then clipped the H_2O contents using the limits specified in Table 1 for sediments, those given by *Jarrard* [2003] for the igneous crust, and the aforementioned three scenarios for the upper mantle section. Hypersolidus phase relations for crustal rocks were determined from the experimental literature (principally from *Schmidt et al.* [2004]). The addition of melting is a signifi-

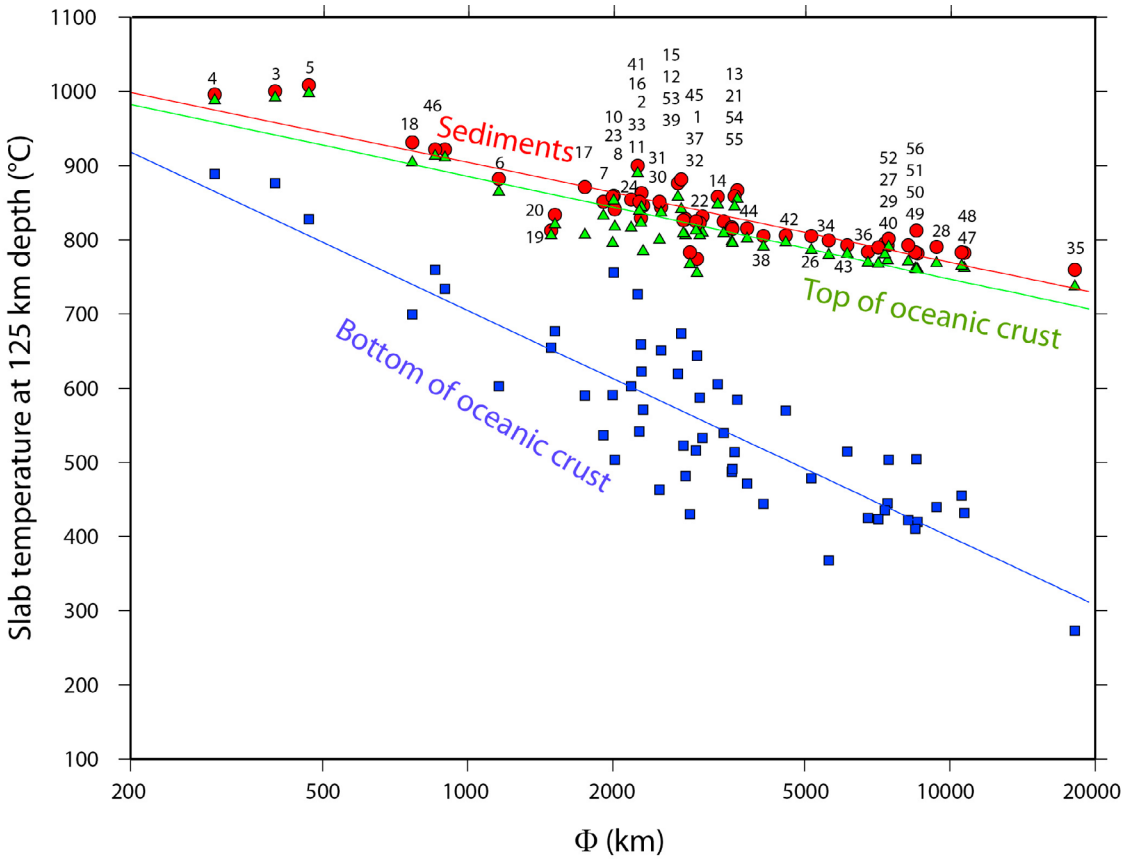

Figure 2. Temperature at three positions in the slab at 125 km depth as a function of the thermal parameter. The temperature is shown at the top of the sediments (red circles), top of the oceanic crust (green triangles), and bottom of the oceanic crust (blue squares; the bottom of the oceanic crust is assumed to be at a constant depth of 7 km below the top of the oceanic crust). Best fits of a function $T = a + b \ln(\Phi)$ are shown in corresponding colors.

cant enhancement of our earlier models and results in more realistic dehydration of crustal lithologies at 700–900°C.

3. Results

3.1. Thermal Structure of Subduction Zones

[12] We summarize the thermal characteristics of the models by showing in Figure 2 the temperature at a depth of 125 km in three locations in the slab (the top of the sediments, the top of the volcanic rocks, and the top of the upper mantle) as a function of the slab thermal parameter Φ [*Kirby et al.*, 1991]. This parameter is defined here as the product of slab age and convergence speed. It is small for slow subduction of young lithosphere (such as at Cascadia) and large for fast subduction of old lithosphere (such as at Tonga). The initial thermal structure has a strong influence on the Moho temperature, which ranges from 200°C to 900°C. At depths of >80 km, the top of the slab drags the mantle wedge down, and the return flow, which is strongly focused due to the temperature- and stress-dependent rheology, causes high slab surface temperatures, with only moderate sensitivity to the thermal parameter. Temperatures at the top of the volcanic section range from 700°C to 1000°C. While the thermal parameter clearly cannot describe the thermal structure of the slab to great precision, it is tempting to provide trend lines. A logarithmic fit for the temperature (in degrees Celsius) at 125 km depth yields

$$T = 1331 - 58.6 \ln \Phi$$

for the top of sediments,

$$T = 1303 - 60.23 \ln \Phi$$

for the top of the volcanic section, and

$$T = 1622 - 132.5 \ln \Phi$$

for the Moho. The Moho fit is similar to that given by *Hacker* [2008], but the top of the slab is significantly warmer in the present models. *Hacker* [2008] used temperature data obtained from a model with the same geometry and parameters as that in the non-Newtonian benchmark (case 2b) of *van Keken et al.* [2008]. The benchmark model predicts lower temperatures due to the simple geometry (constant angle subduction), thick overriding plate (which forms due to the lack of crustal radiogenic heating and assumption of steady state), and lower potential temperature (1300°C instead of 1420°C).

[13] The present thermal models provide a high-resolution temperature distribution, which allows us to more precisely determine the temperature in each compositional layer of the slab. For the thin sedimentary and upper crustal layers we assume that the temperature is that in the center of each layer. The thicker gabbro and uppermost mantle section are divided into 1 km thick layers. The use of more realistic and subduction zone specific models combined with the high-resolution temperature distribution in the slab contributes to significantly more robust predictions of temperature, and therefore of the mineralogy and H_2O content, than those used by *Hacker* [2008].

3.2. Water Distribution in the Slab

[14] From the petrological models we compute the global average H_2O input, weighted by trench lengths. In the case of intermediate (2 wt % H_2O) hydration of the uppermost mantle, we find that 7% of the H_2O in the slab at input is in the sediment, 35% is in the upper crust (volcanic rocks and dikes), 28% is in the lower crust, and 31% is in the mantle. The flux into subduction zones from these models is 10.0 Tg/Myr, which is significantly lower than the value obtained by *Hacker* [2008] and at the lower end of the ranges assumed by previous global compilations (Table 3).

[15] Inspection of the results for individual subduction zones shows a wide variety of patterns of water loss from slabs. Examples of the thermal structure for a hot (Cascadia), intermediate (Nicaragua), and cold subduction zone (Central Honshu) are shown in Figure 3a. The predicted metamorphic facies are shown in Figure 3b. In order to better display the fine details of the crustal and uppermost mantle structure, we transform the coordinates to a slab coordinate system where s is along the slab surface and t is perpendicular to the slab. This allows us to plot the facies with significant vertical exaggeration. The H_2O concentration of the crust and uppermost mantle is shown in Figure 3c.

[16] In Cascadia the full slab dehydrates at relatively shallow depths. The only water source beneath the volcanic arc is predicted to be the serpentinized uppermost mantle which dehydrates by 115 km depth. The entire crust at that depth is hotter than the water-saturated solidus. At greater depths the uppermost volcanic rocks and sediments can potentially carry H_2O again because the solidus bends to a shallower (p, T) slope than the slab surface temperatures. Water fluxed from the serpentinite could potentially rehydrate the uppermost crustal sections.

[17] In the intermediate subduction zone of Nicaragua, we predict that only a small section of the crust is above the water-saturated solidus. Whereas the uppermost crust dehydrates completely below the volcanic front, the deeper (and thus cooler) gabbro can retain H_2O to >230 km depth. Shallower portions of the gabbro and the complete mantle section are predicted to dehydrate below ~150 km depth, suggesting that H_2O can be sourced from the slab at variable depths beyond the volcanic front. This prediction is consistent with Cl-isotope evidence for fluids being derived from serpentinite in the Nicaragua arc [*Barnes et al.*, 2009] and the seismic evidence for significant serpentinization of the mantle due to normal faulting in the fore-arc high [*Ranero et al.*, 2003; *Ivandic et al.*, 2008]. Dehydration of much of the crust below the hot wedge here agrees with changes in observed boundaries in migrated scattered wave imaging [*MacKenzie et al.*, 2010].

[18] For a cold subduction zone such as Central Honshu, we find that the uppermost crust dehydrates below the volcanic front, but that the entire lower crust and uppermost mantle have significant water-carrying capacity to profound depths. The location of the main dehydration reactions here is consistent with the location of in-slab seismicity [*Kita et al.*, 2006] and the position of the low velocity layer seen in seismic tomography [*Nakajima et al.*, 2009].

[19] We further note good agreement between our predicted slab surface temperature over a significant depth range for Kamchatka with the H_2O/Ce derived temperatures of fluid release by *Plank et al.* [2009], who provide an explicit comparison between the geochemistry and the regional thermal model in their Figure 4. The predicted slab surface temperature for the Antilles is also in good agreement with the range inferred by comparing trace element geochemistry with experiments on clay melting [*Skora and Blundy*, 2010].

[20] The various layers in a subducting slab have different bulk compositions that lead to differences in mineralogy and thus in how much H_2O is carried as a function of p and T. The layers also experience different (p, T) paths as a result of their different positions in the slab. The end result is that the magnitude and depths of H_2O loss can vary dramatically from layer to layer. Figure 4 illustrates this using the (intermediate) southern Mariana subduction zone as example. The sediment at the top of the slab experiences high temperatures and reaches H_2O-saturated melting conditions over a narrow depth range of ~80–120 km, but the position and shape of the H_2O-saturated solidus imply that ~1 wt % H_2O can still be retained to depths of >200 km. The volcanic hypabyssal section of the ocean crust is slightly cooler (Figure 4b), but the lower K_2O content destabilizes hydrous phases, resulting in lower (<1 wt %) H_2O content than that of the sediments. The gabbro has an even lower H_2O content but is cold enough that it undergoes no H_2O loss to depths

Figure 3. Cross sections of predictions for (a) temperature, (b) metamorphic facies, and (c) water content for Cascadia, Nicaragua, and Central Honshu as representatives for cold, intermediate, and hot subduction zones. Note the variable horizontal scale in Figure 3a. To display the facies and water content more clearly in the slab, we project the coordinates into a slab reference frame with s parallel to the slab and t perpendicular to the slab. The lower two rows show the facies and water content in this reference frame. The labels "80," "100," and "150" indicate the locations where these depths (in km) are reached. "hb sol," hornblende solidus; "H_2O-sat'd sol," H_2O-saturated solidus. The composition and temperature of the slab strongly influence the metamorphic facies and therefore H_2O-carrying capability. Cold slabs such as Central Honshu can retain H_2O to large depths, whereas warm slabs such as Cascadia dehydrate completely. Intermediate subduction zones such as Nicaragua show dehydration at various depth levels but have significant H_2O-carrying capacity in the gabbros.

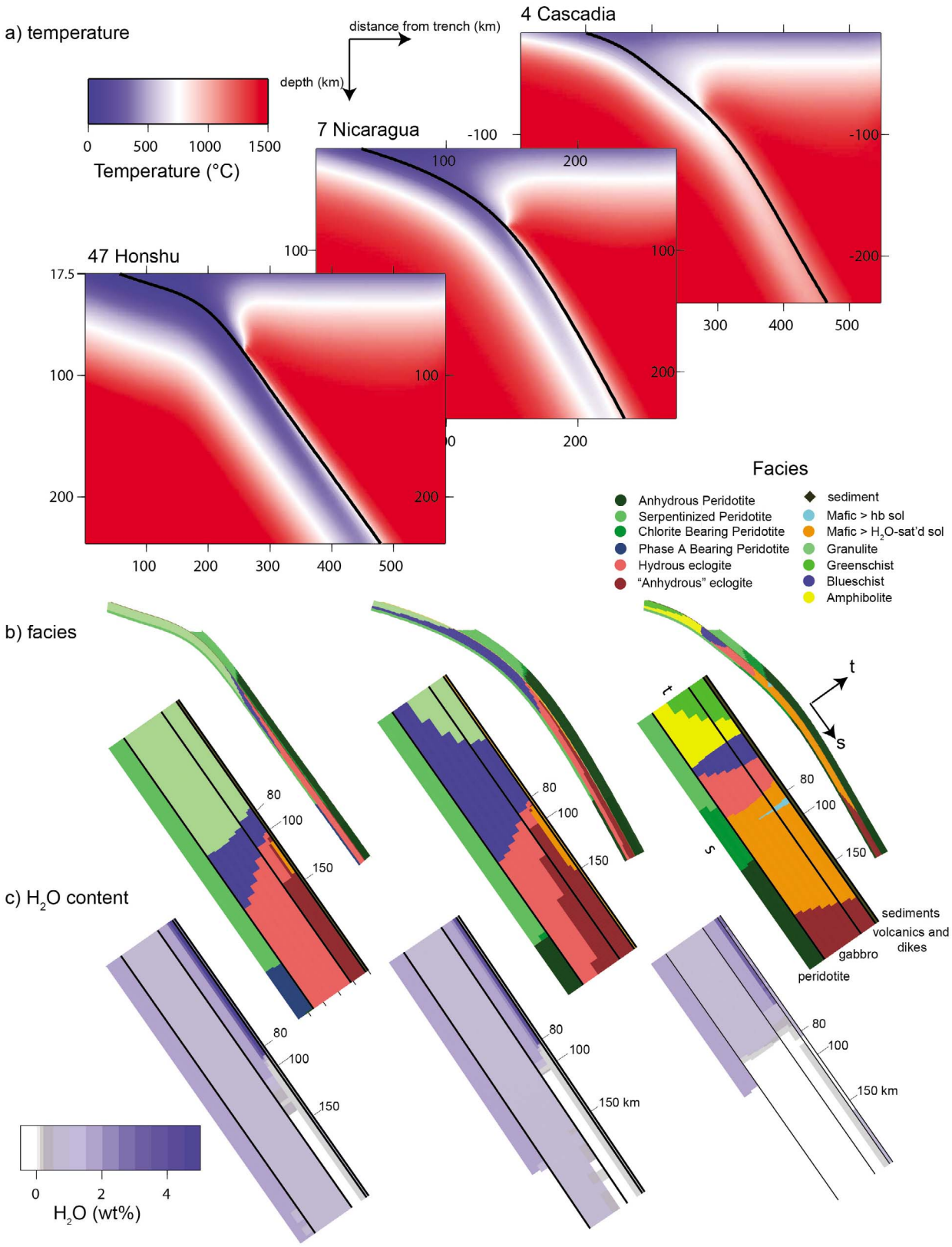
a) temperature
distance from trench (km)
depth (km)
0 500 1000 1500
Temperature (°C)
4 Cascadia
7 Nicaragua
47 Honshu
Facies
Anhydrous Peridotite
Serpentinized Peridotite
Chlorite Bearing Peridotite
Phase A Bearing Peridotite
Hydrous eclogite
"Anhydrous" eclogite
sediment
Mafic > hb sol
Mafic > H2O-sat'd sol
Granulite
Greenschist
Blueschist
Amphibolite
b) facies
c) H2O content
t
s
sediments
volcanics and dikes
gabbro
peridotite
80
100
150
150 km
0 2 4
H2O (wt%)

Figure 3

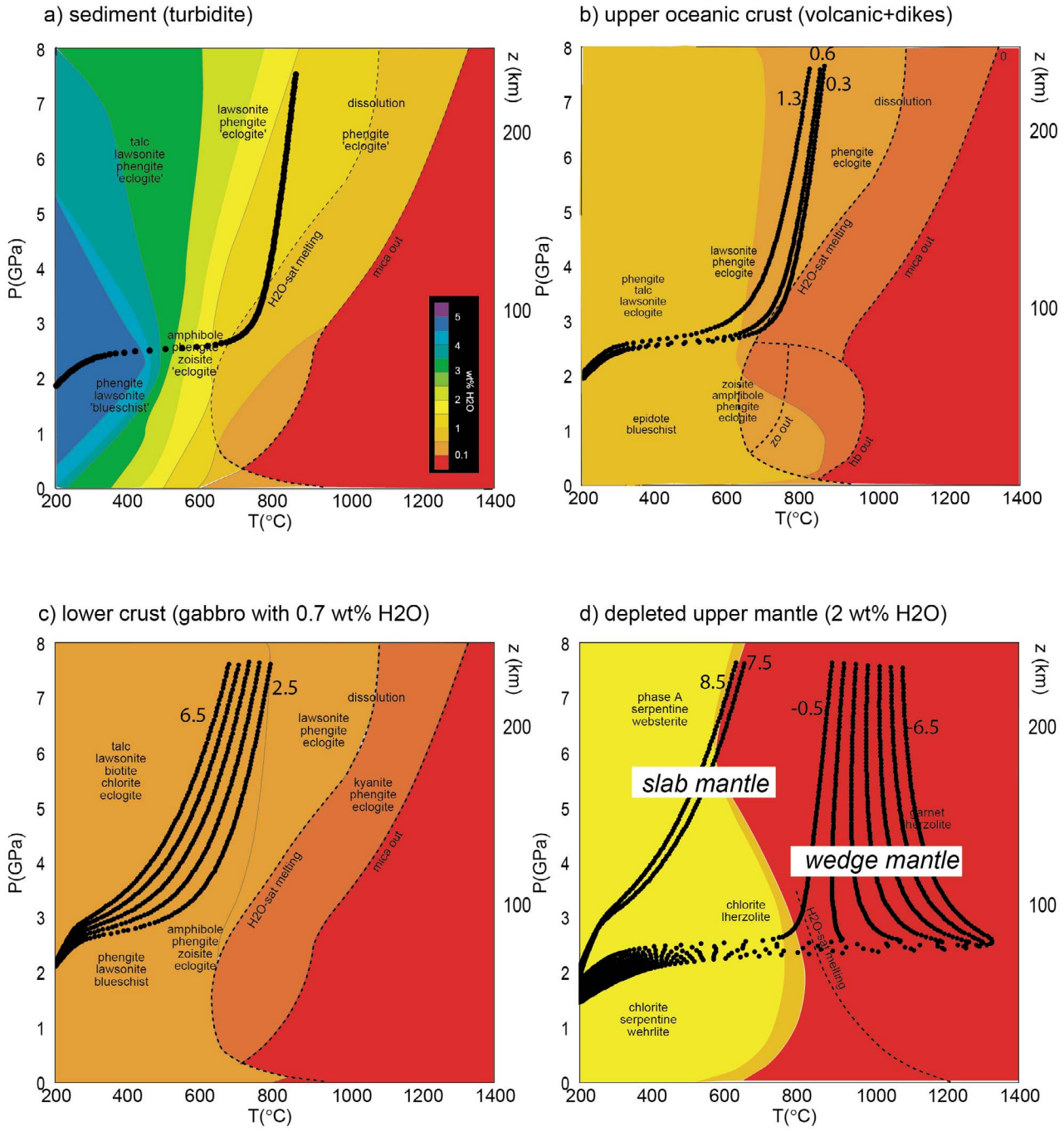

Figure 4. Example of (p, T) paths for the southern Mariana subduction zone in and directly on top of the slab compared to the representative phase diagrams. The pressure-temperature curves are derived from the thermal model for paths that run parallel to the top of the slab. The numbers next to the $p - T$ paths indicate the depth in km below sediments (positive numbers) or the height in km above the sediments (negative numbers). The phase diagrams vary as a function of lithology at various depths in the slab. (a) The $p - T$ path in the middle of sediments (modeled here as turbidite). (b) The $p - T$ paths in the uppermost 2 km of the oceanic crust. (c) The $p - T$ paths in lowermost 5 km of the oceanic crust. (d) The $p - T$ paths in the slab mantle (to 2 km below Moho) and wedge mantle (to 6.5 km above the slab). In general, sediments reach the H_2O-saturated solidus, but the high-temperature gradients allow parts of the volcanic crust and gabbros to retain H_2O. The wedge mantle is in all cases too hot to retain hydrated phases. The serpentinized upper mantle below the crust is expected to be dehydrated in all but the coldest subduction zones.

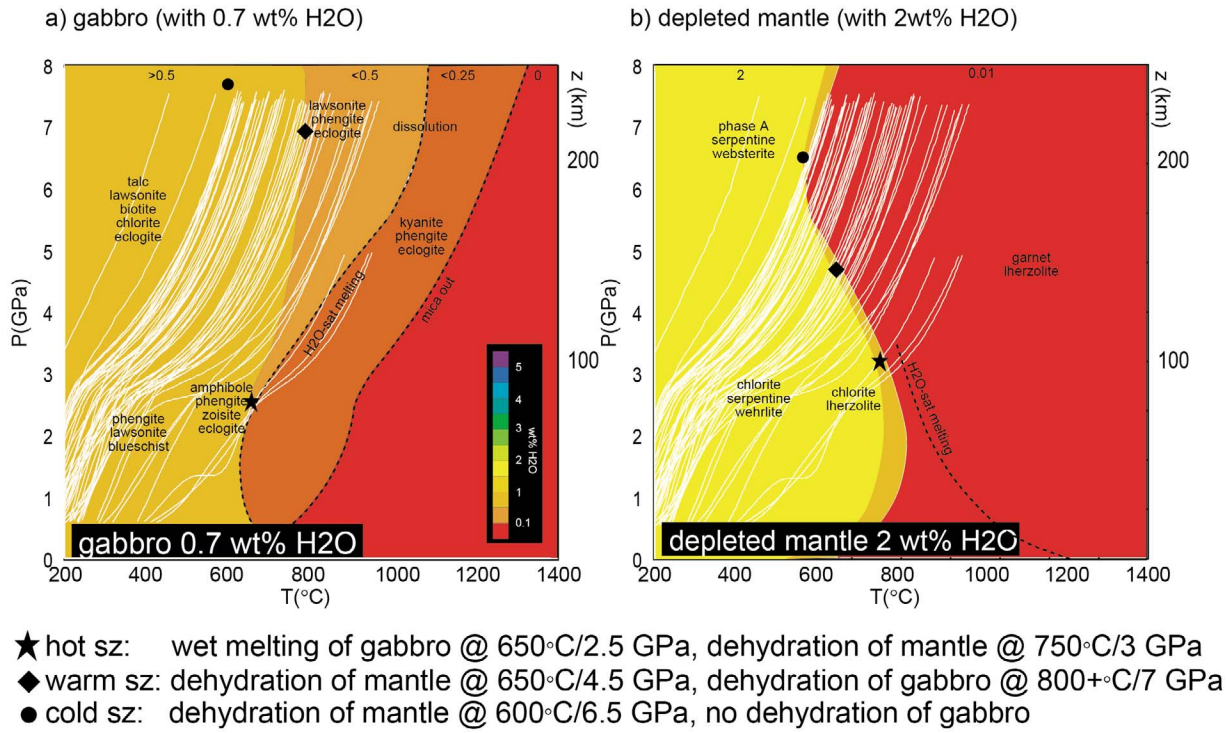

Figure 5. Moho (p, T) paths for global subduction zones on phase diagrams of (a) gabbro and (b) depleted mantle highlight the variation in subduction zone dehydration. In some cold subduction zones (circle) the slab mantle can undergo dehydration around 200 km depth due to the loss of chlorite, whereas H_2O is retained in the gabbros to larger depths. In intermediate subduction zones (diamond) dehydration of the mantle is complete by ~150 km whereas only minor dehydration occurs in the gabbros. In hot subduction zones (star) dehydration of the mantle is complete by ~100 km depth and significant dehydration of the gabbros from the breakdown of K-white mica has occurred at depths as shallow as 80 km.

of 200 km (Figure 4c). The wedge mantle (Figure 4d) is the hottest part of the system at any given depth and is effectively completely dehydrated due to the breakdown of chlorite at ~800°C and ~80 km depth.

[21] From these results we see that dehydration in subduction zones follows a general pattern that depends strongly on position in the slab.

1. The top of the sediments typically reaches H_2O-saturated melting conditions but only for a narrow depth range. Unless phengite breaks down completely, which requires considerably higher temperatures, subducting sediment can retain H_2O to at least 200 km depth.

2. The upper oceanic crust sees a strong temperature gradient, such that the upper volcanic rocks may undergo H_2O-saturated melting below the volcanic arc, whereas the underlying dikes may retain H_2O to at least 200 km.

3. Except in the youngest subduction zones the gabbro section is sufficiently cool for lawsonite and phengite to remain stable.

4. Hydrous phases are unstable in the overlying mantle wedge at relatively shallow depths; it is only the cold wedge tip below the fore arc that can be hydrated. We predict that the uppermost mantle in most slabs will dehydrate between 100 and 200 km depth.

5. In warm subduction zones, the entire slab crust and uppermost mantle become anhydrous at shallow to moderate depths, whereas in cold subduction zones, the cold core of the slab can carry H_2O to >200 km in gabbro and peridotite.

3.3. Global Comparison of H_2O Loss

[22] Cold slabs show dehydration behavior that is markedly different from that of warm slabs. The reason for this is illustrated in Figure 5, which shows that the main dehydration reactions for mafic rocks have steep, positive Clapeyron slopes, whereas the main dehydration reactions for depleted mantle have steep negative slopes at <200 km. Only in the hottest subduction zones do the basal gabbros become hot enough to dehydrate. Most subduction zones can carry significant water to >7 GPa (Figure 5a). In contrast, only in the coldest subduction zones can the uppermost mantle carry H_2O to any significant depth (Figure 5b). This occurs in the central portion of the Indonesian arc, Tonga-Kermadec, south Philippines, Marianas, and the Tohoku-Kamchatka trench.

[23] There is considerable variation in the magnitude and depth of H_2O loss from slabs (Figure 6 and Table 2). A few warm slabs show considerable H_2O loss at depths of 50–80 km. Most slabs, however, produce a large burst of fluid around 80 km depth, where the thermal models assume that the overlying mantle wedge couples to the slab. Beyond ~100 km depth, some slabs show relatively continuous H_2O

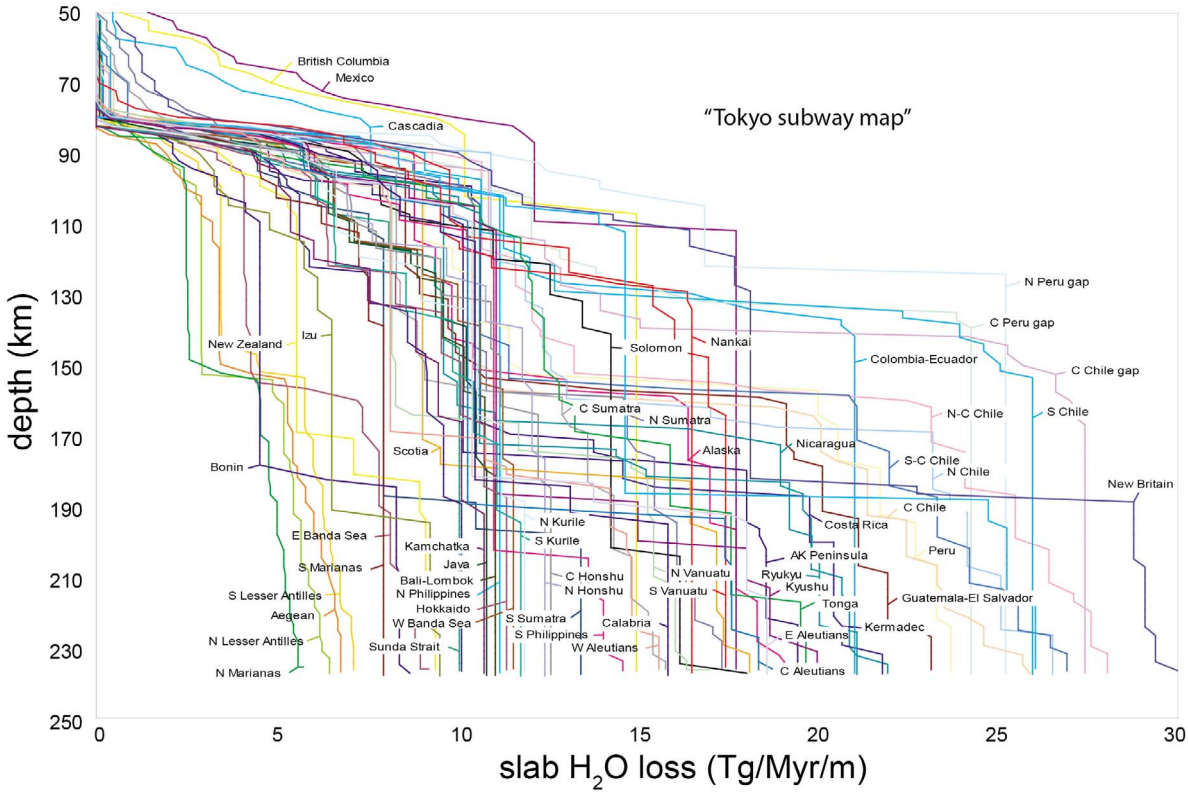

Figure 6. Diverse H_2O loss as function of depth in each subduction zone. The hottest subduction zones lose significant H_2O in the fore arc. All subducting slabs lose significant water as soon as the slab gets into contact with the hot overlying mantle wedge (modeled here to be at 80 km depth). For many slabs (e.g., Kamchatka, Calabria) further dehydration is minor. Other slabs (e.g., Chile) continue to dehydrate significantly with increasing depth principally due to the dehydration of the uppermost mantle. A few slabs (e.g., Marianas) are so cold that little H_2O is lost even at 230 km depth.

loss with depth, whereas others show distinct pulses in H_2O loss.

[24] The bulk of the modeled H_2O loss comes from the slab igneous rocks in most subduction zones. H_2O loss from sediments is relatively similar from one arc to the next and considerably smaller in magnitude than other sources. H_2O loss from the slab mantle does not occur until greater depths; the magnitude of this loss is a strong function of the assumed hydration state of the slab mantle.

[25] From this set of models we can compute a global average of the flux of H_2O at various depths (Table 3 and Figure 7). At 15 km depth we calculate 10.0 Tg/Myr entering subduction zones (carried by upper crust/lower crust/mantle in the ratio 41%/28%/31%). From 15 to 100 km depth, 3.2 Tg/Myr H_2O is released from slabs globally, principally by dehydration of the upper crust, leading to a global flux of 6.8 Tg/Myr beyond 100 km depth (distributed in the ratio 17%/38%/45%). In the depth range 100–150 km the flux is reduced by a further 1.4 Tg/Myr to 5.4 Tg/Myr (9%/43%/48%). The dehydration from 150 to 230 km is 2.0 Tg/Myr and is dominated by release from the slab mantle, leading to a global H_2O subduction flux of 3.4 Tg/Myr (9%/54%/36%) to depths >230 km.

[26] These estimates are based on the assumption that the upper crust rehydrates after crossing the H_2O-saturated solidus (Figure 4a). This assumption affects the predicted flux of H_2O only in the hottest subduction zones and causes an insignificant (1%) increase in the flux to the wedge below 100 km.

4. Discussion

4.1. Sensitivity of Global Fluxes to Model Assumptions

[27] The dehydration estimates provided in this paper are sensitive to the thermal structure and the assumed hydration state of the incoming crust and mantle. The thermal structure is most strongly affected by the age and speed of the subducting slab (which we consider relatively robust for the subduction zones considered here), the potential temperature, the nature of coupling between slab and mantle, the rheology of the overriding plate, and temporal variations in slab parameters. Like *Syracuse et al.* [2010], we chose a potential temperature T_p = 1421.5°C based on the GDH1 plate model of *Stein and Stein* [1992]. While this value is reasonable for some arcs (e.g., Izu [*Tollstrup et al.*, 2010]), considerable variation is suggested for a number of back arcs [*Wiens et al.*, 2006]. We evaluated the influence of variations in T_p (ΔT_p) for a number of subduction zones and found that as a rule of thumb the effect is strongest at the top of the slab, which sees a change of $\Delta T_p/2$ with a

Table 2. Characteristics of Subduction Zone Models

Zone	Location	Longitude (deg)	Latitude (deg)	Speed (mm/yr)	Age (Ma)	Length (km)	Sediment (km)	H_2O Flux (With Serpentinization) (Tg/Myr/m)				H_2O Flux (No Serpentinization) (Tg/Myr/m)				H_2O Flux (Full Serpentinization) (Tg/Myr/m)			
								Input	100 km	150 km	230 km	Input	100 km	150 km	230 km	Input	100 km	150 km	230 km
1	Alaska Peninsula	−153.6	58.9	59	52.2	510	0.4	26.0	15.2	15.4	5.4	18.4	7.6	7.7	5.4	53.0	42.3	31.1	5.4
2	Alaska	−158.8	56.5	49	47	610	0.4	21.6	12.4	10.8	1.3	15.2	6.1	4.5	1.3	44.0	34.8	10.9	1.3
3	British Columbia	238.5	42.0	40	10	625	0.4	15.5	5.2	0.0	0.0	10.4	0.0	0.0	0.0	26.7	5.1	0.0	0.0
4	Cascadia	238.0	47.0	30	10	450	0.4	11.6	1.9	0.0	0.6	7.7	0.0	0.0	0.6	19.9	1.9	0.0	0.6
5	Mexico	260.5	19.1	47	10	1350	0.3	18.4	6.1	0.0	0.6	12.4	0.0	0.0	0.6	32.0	6.5	0.0	0.6
6	Guatemala-El Salvador	−90.4	14.2	67	17.4	500	0.3	25.7	16.6	14.3	0.6	17.1	7.9	5.7	0.6	56.2	44.5	14.5	0.6
7	Nicaragua	−86.7	12.5	71	27	580	0.3	27.9	18.0	17.7	5.2	18.8	8.8	8.6	5.2	60.3	50.4	36.5	5.2
8	Costa Rica	−84.7	10.5	75	27	280	0.3	29.5	21.4	18.7	6.0	19.8	11.7	9.1	6.0	63.7	55.6	38.6	6.0
9	Columbia Ecuador	−77.5	0.0	60	15	900	0.3	22.8	11.9	0.1	0.2	15.0	4.2	0.1	0.2	48.4	28.0	0.1	0.2
10	N Peru	−79.0	−6.8	69.5	29	850	0.4	27.5	12.4	0.1	0.2	18.6	3.4	0.1	0.2	59.3	23.8	0.1	0.2
11	C Peru	−76.8	−11.2	66.7	33.9	900	0.4	26.5	15.1	0.1	0.2	17.9	6.5	0.1	0.2	57.0	35.7	0.1	0.2
12	Peru	−70.9	−16.6	65.1	42.1	500	0.4	25.9	16.2	13.0	0.2	17.5	7.8	4.8	0.2	55.7	46.0	12.4	0.2
13	N Chile	−68.6	−20.8	79	46.1	460	0.2	31.3	19.7	17.8	2.6	21.1	9.4	7.6	2.6	67.5	55.9	28.6	2.6
14	NC Chile	−68.5	−24.7	77.4	42.8	490	0.2	30.6	19.3	16.7	0.7	20.6	9.3	6.7	0.7	66.1	54.7	17.1	0.7
15	C Chile 1	−69.5	−30.0	73.8	37.7	640	1.3	30.1	18.6	1.3	0.4	20.6	9.1	1.3	0.4	63.8	52.4	1.3	0.4
16	C Chile 2	−70.6	−35.2	71.6	32.4	500	1.3	29.1	20.7	17.3	1.3	19.9	11.4	8.1	1.3	61.8	53.3	17.9	1.3
17	SC Chile	−72.8	−43.8	74.7	23.5	490	1.3	29.9	19.1	18.0	0.9	20.3	9.4	8.4	0.9	64.0	51.7	18.2	0.9
18	S Chile	−71.7	−39.5	74.9	10.3	360	0.6	27.9	16.5	1.1	0.3	18.3	6.9	1.1	0.3	49.6	38.0	1.1	0.3
19	N Antilles	−61.7	16.1	17.6	85	430	0.25	7.5	4.5	4.4	0.8	5.2	2.4	2.2	0.8	15.6	12.3	1.3	0.2
20	S Antilles	−61.2	13.3	17.9	85	430	0.5	8.2	4.6	3.5	0.5	5.9	2.3	2.3	0.5	16.4	9.9	1.4	0.3
21	Scotia	−26.5	−57.8	60.8	59.1	700	0.2	24.9	15.3	15.5	5.4	17.0	7.4	7.6	5.4	52.9	43.3	35.3	5.4
22	Aegean	25.4	36.4	15	200	1200	1	7.7	4.1	4.2	0.5	5.8	3.3	2.3	0.5	14.6	10.7	1.8	0.5
23	N Sumatra	97.6	3.9	41.5	48.3	760	1.4	22.2	11.8	12.6	3.8	16.8	6.4	7.2	3.8	41.1	30.7	12.8	3.8
24	C Sumatra	100.0	0.1	40	54.8	600	0.85	19.2	10.7	9.8	2.9	14.0	5.5	4.6	2.9	37.5	29.0	10.0	2.9
25	S Sumatra	102.4	−3.4	48.7	70	650	0.3	20.8	12.6	12.8	6.5	14.5	9.2	6.5	6.5	43.1	35.0	25.7	4.7
26	Sunda Strait	106.7	−6.8	61	85	605	0.3	26.3	17.7	15.8	16.5	18.5	12.4	7.9	8.6	54.4	45.7	41.1	7.9
27	Java	111.8	−7.8	67.8	110	605	0.3	29.1	21.7	19.0	17.8	20.3	13.9	10.2	9.0	60.2	52.8	48.9	18.3
28	Bali-Lombok	116.5	−8.4	69.8	135	640	0.3	29.9	22.3	19.6	18.3	20.9	14.3	10.5	9.3	62.0	54.4	50.3	18.9
29	W Banda Sea	121.8	−8.8	73.6	100	780	0.2	31.0	23.2	20.2	19.4	21.5	14.8	10.7	9.9	64.8	57.1	52.6	21.8
30	E Banda Sea	129.5	−6.7	25.3	100	1065	0.2	10.7	6.4	6.3	1.1	7.4	3.1	3.0	1.1	22.3	17.6	1.8	0.2
31	New Britain	150.9	−5.5	100.4	25	690	0.6	45.1	34.2	27.6	13.9	32.2	21.2	14.6	13.3	91.1	80.2	69.4	13.8
32	Solomon	154.9	−5.8	93.6	31	450	0.2	39.0	31.0	24.3	23.4	26.9	18.9	12.2	11.9	81.9	74.0	67.3	21.7
33	N Vanuatu	167.5	−13.8	51.8	44	760	0.2	21.7	13.1	12.9	4.6	15.0	6.3	6.2	4.6	45.5	36.9	26.7	4.6
34	S Vanuatu	169.8	−20.2	112.7	50	850	0.2	47.2	37.3	29.3	28.9	32.6	22.7	14.7	14.3	99.1	89.2	81.2	39.8
35	Tonga	−174.9	−19.2	165.8	110	1110	0.2	68.4	56.0	56.0	47.7	46.9	37.6	34.5	26.2	144.8	132.4	127.2	119.5
36	Kermadec	−178.5	−30.2	64.6	105	1545	0.2	27.3	21.4	17.7	16.7	19.0	13.7	9.3	8.4	57.1	51.2	46.3	18.3
37	New Zealand	177.0	−37.9	30.4	100	800	0.4	13.5	7.8	8.0	4.0	9.6	4.0	4.1	4.0	27.5	21.7	12.0	2.2
38	S Philippines	125.5	9.6	69	59.8	1750	0.2	28.9	21.8	17.6	17.2	20.0	12.8	8.7	8.7	60.6	53.4	49.3	19.1
39	N Philippines	120.6	16.3	87.7	32.4	740	0.3	37.4	25.3	22.6	9.8	26.1	14.0	11.3	9.8	77.5	65.5	55.5	9.8
40	S Marianas	145.8	17.6	50	150	500	0.2	21.2	13.1	13.0	12.8	14.7	9.6	6.5	6.5	44.2	36.1	33.8	6.6
41	N Marianas	143.4	21.9	15.3	150	500	0.2	6.5	3.9	2.8	0.4	4.5	1.9	1.8	0.4	13.5	10.4	1.1	0.1
42	Bonin	140.9	27.2	31.6	145	630	0.2	12.8	7.9	7.9	3.8	8.7	5.1	3.8	3.8	27.3	22.5	16.4	2.7
43	Izu	139.8	33.1	45.6	135	680	0.2	18.4	13.3	11.7	8.6	12.5	8.7	5.8	5.5	39.4	34.3	26.3	4.9
44	Kyushu	130.6	31.2	72	53	550	0.2	29.9	20.8	18.6	8.5	20.6	11.5	9.3	8.1	62.9	53.9	51.4	8.5
45	Ryukyu	128.3	27.9	69.5	43	1090	0.2	28.7	17.9	17.9	6.1	19.8	8.9	8.9	6.1	60.6	49.7	40.0	6.1
46	Nankai	137.3	35.3	43	20	520	0.3	17.9	7.7	0.3	0.5	12.3	2.2	0.3	0.5	37.4	19.1	0.3	0.5

Table 2. (continued)

Zone	Location	Longitude (deg)	Latitude (deg)	Speed (mm/yr)	Age (Ma)	Length (km)	Sediment (km)	H_2O Flux (With Serpentinization)			H_2O Flux (No Serpentinization) (Tg/Myr/m)			H_2O Flux (Full Serpentinization) (Tg/Myr/m)		
								Input	100 km	150 km	230 km	Input	100 km	150 km	230 km	Input	100 km	150 km	230 km
47	C Honshu	140.3	37.6	82.7	130	530	0.3	34.5	27.3	22.7	21.2	23.8	16.7	12.0	10.5	72.5	65.3	59.2	21.9
48	N Honshu	140.9	40.7	81.6	130	250	0.3	34.0	25.8	22.4	20.9	23.5	16.5	11.9	10.4	71.5	63.3	58.2	14.4
49	Hokkaido	147.0	44.6	74.7	115	450	0.3	31.1	24.7	20.5	19.2	21.5	15.6	10.9	9.5	65.5	59.0	53.8	21.0
50	S Kurile	151.8	46.8	77.4	110	510	0.3	32.2	25.5	22.7	19.9	22.2	16.1	12.7	9.9	67.8	61.1	55.8	26.5
51	N Kurile	155.4	50.3	78.3	105	570	0.3	32.6	25.8	21.5	20.1	22.5	15.8	11.4	10.0	68.6	61.8	56.0	25.7
52	Kamchatka	159.2	53.6	75.1	95	530	0.3	30.2	24.7	20.2	18.8	20.5	15.0	10.5	9.1	64.7	59.2	53.3	24.2
53	W Aleutians	−178.8	51.8	50.2	56.1	1650	0.3	21.3	13.0	13.1	4.6	14.8	6.5	6.7	4.6	44.4	36.1	26.5	4.6
54	C Aleutians	−172.5	52.3	63.4	55.9	360	0.3	26.9	18.5	16.6	7.4	18.7	10.3	8.4	7.4	56.1	47.6	42.8	7.4
55	E Aleutians	−166.0	54.1	64.2	55.3	610	0.3	27.3	18.7	16.8	7.5	19.0	10.4	8.5	7.5	56.8	48.2	43.3	7.5
56	Calabria	15.0	38.5	45	190	400	1	23.4	15.1	12.8	8.9	17.6	9.7	6.9	8.6	44.2	35.9	27.4	8.0

Table 3. Estimates of Subduction Zone Water Flux (in 10^8 Tg/Myr)[a]

	P90	B95	J03	SP03	R04	H08	This Study w s	This Study w/o s
Bound H_2O input								
Sediment	0.7	0.3–1.4	1.2		1.6	1.5	0.7	0.7
Igneous crust	8	9–18	6		4.6	6.1	6.3	6.3
Mantle				4.9–8.6	2.4–12	5.7	3.0	0
Total input	8.7	9–19		9–12	9–18	13	10.0	7
Subduction zone H_2O loss								
To 100 km depth				4.8–7.5			3.2	3.2
100–150 km				1.8–8.0			1.4	1.0
150–230 km				1.6–3.6			2.0	0.6
>230 km				0–10			3.4	2.2

[a]P90, *Peacock* [1990]; B95, *Bebout* [1995]; J03, *Jarrard* [2003]; SP03, *Schmidt and Poli* [2003]; R04, *Rüpke et al.* [2004]; H08, *Hacker* [2008]; w s, with 2 km of serpentinized upper mantle (2 wt %); w/o s, without hydrated upper mantle.

strong further reduction in temperature change as one descends into the slab crust. A globally lower T_p would therefore have the strongest influence on the sediment and volcanic rocks and lead to slightly higher recycling rates. We investigated various models for slab coupling [*Syracuse et al.*, 2010] and compared our results with those obtained with an independent formulation [*Wada and Wang*, 2009]. While the differences in coupling approach can lead to significant differences in the depth at which the slab couples, the temperature increase remains uniform once the slab fully couples, and we consider the impact of the coupling formulation minimal. The rheology of the wedge will have a stronger influence. The presence of fluids in the wedge may reduce the viscosity significantly, which should lead to stronger wedge flow and higher slab surface temperature at least near the coupling point [e.g., *Billen et al.*, 2003; *Currie and Hyndman*, 2006; *Arcay et al.*, 2007]. This will have the strongest effects on the top of the slab but little effect on the deeper layers except in very slow subduction zones. Since the upper crust is already significantly dehydrated, we expect that the total H_2O-carrying capability of the slab will be reduced somewhat, but there will be limited influence on the concentrations in the lower crust and upper mantle. Finally, temporal variations in slab input parameters and trench rollback or advance may change the wedge flow and cause changes in the slab surface temperature [e.g., *Lee and King*, 2010; *Jadamec and Billen*, 2010]. These tend to shift the slab surface temperature to higher values, and by a similar argument as with the rheological uncertainty we expect only a small reduction in H_2O-carrying capability. We finally note that our model has the common assumption that the incompressible flow equations can be used. *Lee and King* [2009] explicitly tested this assumption and found that the effects of including compressibility are negligible in this type of subduction modeling.

[28] In comparison to thermal structure we find considerably more sensitivity of the H_2O recycling efficiency to the model assumptions of the hydration state of the slab. The degree to which it is necessary to know the hydration state of the incoming slab depends on the depth interval over which one wishes to understand the H_2O flux, because different layers of the slab experience different temperatures and grow different metamorphic minerals. For example, at

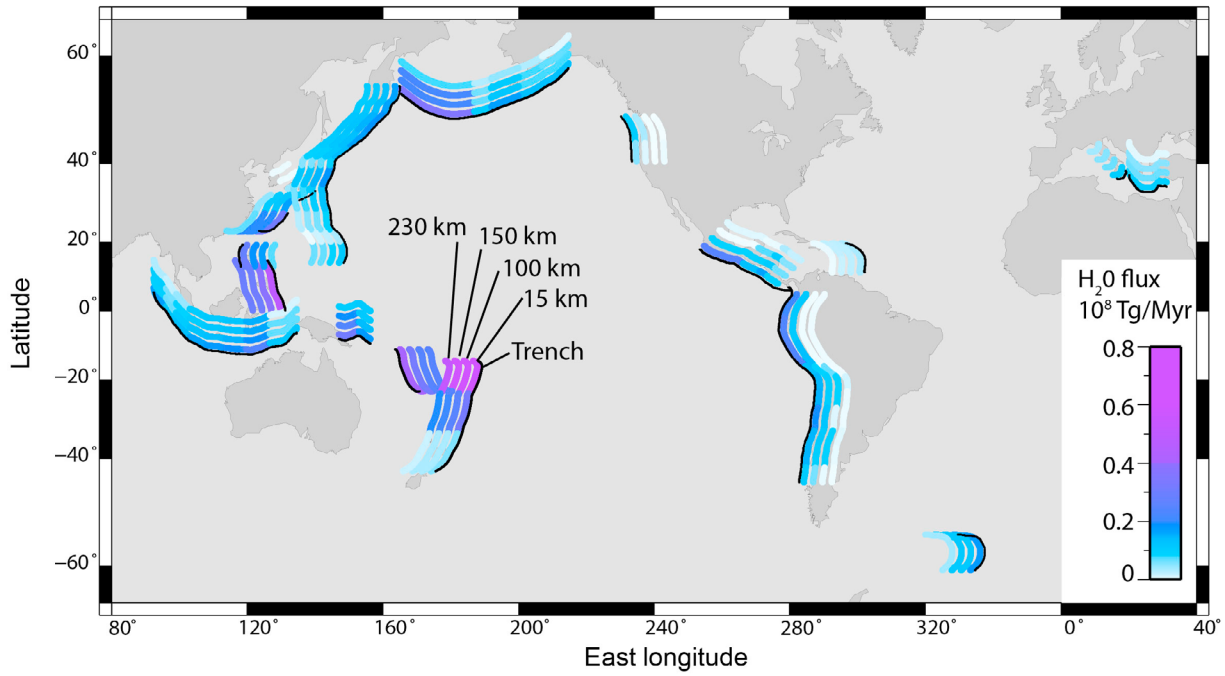

Figure 7. Predicted H_2O flux at selected depths in the world's subduction zones. For each subduction zone the black line indicates the position of the trench. The parallel lines in the direction of subduction show H_2O input to the fore arc (at 15 km depth), H_2O flux at the approximate location of the volcanic front (at 100 km depth), H_2O flux at 150 km depth, and H_2O input to >230 km depth, respectively.

about 200 km depth in a typical subduction zone nearly all the H_2O has been driven from the uppermost slab mantle and the uppermost crust, whereas the amount of H_2O subducted beyond 200 km depends more on the hydration state of the lower crust.

[29] The constraints on H_2O content of the sediments and volcanic rocks may be more robust than the deeper slab layers, but we have still made important assumptions. We have assumed one of six types of sediment composition, whereas subducting sediment varies in composition in three dimensions, even in individual subduction zones. We use the model of *Jarrard* [2003] to describe the hydration state of the igneous oceanic crust. This model is based on widespread drill cores but does not include extreme sites of alteration, such as at transform faults, which might even provide the bulk of subducted H_2O. In addition, few drill cores penetrate the gabbros that make up most of the oceanic crust and uncertainties in hydration state of the lower crust are considerably bigger than that of the volcanic rocks. The H_2O concentration of the upper mantle has likely the largest uncertainty because of the variable influence of features such as transform faults, oceanic core complexes, and the unknown degree, depth, and localization of hydration that accompanies bending at the outer rise. Geophysical observations suggest that the depth to which the mantle can be hydrated is significantly larger than what is assumed here [*Ivandic et al.*, 2008; *Lefeldt et al.*, 2009], but evidence for mantle hydration is as yet limited to only a few subduction zones. Our assumption of 2 km hydration by 2 wt % H_2O is likely too small for subduction zones such as Nicaragua, but it is considered to be a reasonable global average. To help assess the sensitivity of our assumption, in Table 2 we provide H_2O fluxes for our base assumption and for those of zero and full hydration of the uppermost mantle. The global flux resulting from the assumption that the upper mantle is dry or fully hydrated is shown in Table 3. In the dry case, the total flux to the deep mantle is reduced by about 60% to 2.2×10^8 Tg/Myr and is principally carried in the gabbro. In the full hydration case the deep mantle flux is increased by about 25% to 4.3×10^8 Tg/Myr.

4.2. Perspectives on the Dehydration of the Slab and Consequences for the Global Water Cycle

[30] With our base assumption of the H_2O content of the average slab, we find that the slab as a whole dehydrates by 66% at 230 km depth. This reflects significant water loss, but is substantially lower than the 97% dehydration estimate for slab crust inferred by *Dixon et al.* [2002]. Their 97% dehydration rate is based on the low water concentration in Alpine anhydrous eclogites with ~600 ppm H_2O [*Nadeau et al.*, 1993] and led *Dixon et al.* [2002] to suggest that the moderately high water content inferred for the mantle plume source does not come from slabs, but has a juvenile origin. Our modeling shows that the downgoing oceanic crust can retain significant lawsonite and phengite and that therefore anhydrous eclogites are not a good analog for average subducting oceanic crust. This alleviates the need for a juvenile origin of water in the plume source. We find that 89% of H_2O in the upper crust is lost, which is in reasonable agreement with the value obtained by *Dixon et al.* [2002] which was based on a comparison of water concentrations inferred for enriched mantle (EM) plumes with estimates of global sedimentary input [*Plank and Langmuir*, 1998].

[31] A different estimate for slab dehydration comes from the analysis of hydrogen isotopes (δD). *Shaw et al.* [2008] showed by comparing the δD of fluid inclusions in the North and Central Mariana subduction zone with that of the average upper mantle that the slab must undergo significant dehydration (88%). This is in good agreement with our model estimates suggesting the slab below this arc nearly completely dehydrates.

[32] Our estimate of the global H_2O input from the subducting slab into the fore-arc region is 10×10^8 Tg/Myr, which is at the lower range of recent compilations [*Jarrard*, 2003; *Schmidt and Poli*, 2003; *Rüpke et al.*, 2004]. While minor H_2O release occurs in the fore arc, the bulk of water is expelled from the sediments and upper crust below the volcanic front with progressive further dehydration of the deeper layers at larger depths (Figure 6). While fluid pathways in the wedge are not clear and the relative partitioning of released fluids into the cold fore arc, volcanic front, and deeper wedge mantle is uncertain, we find that our estimate of 3.3×10^8 Tg/Myr loss to 100 km depth is in good quantitative agreement with the estimate of global arc loss of *Wallace* [2005] (3×10^8 Tg/Myr). This represents 33% of total dehydration of the slab. Another 35% of the input is lost below the volcanic arc due to progressive dehydration down to 230 km depth. The incomplete dehydration leads to a flux of 3.2×10^8 Tg/Myr of H_2O into the underlying mantle. Most of this is carried by peridotite (36%) and plutonic crust (54%). The lower recycling rate to the deep mantle is principally due to the lower H_2O content of the slab mantle that we assumed here, with a minor influence of the high slab surface temperature in these models. The recycling rate to the deeper mantle is still significant and corresponds to an influx of about one ocean mass over the age of the Earth. This would increase the mantle H_2O concentration by 0.037 wt % (370 ppm).

[33] Our present-day estimate for the subduction efficiency (i.e., the proportional amount of H_2O that passes the subduction zone filter) is 32%. It is reasonable to assume that the estimated present-day flux is significantly higher than the average over the age of the Earth. Secular cooling of the Earth likely made the recycling of water far less efficient because a larger amount of water would be released at shallower depths, even if subduction itself was not less efficient due to the higher temperature of the upper mantle [*Vlaar et al.*, 1994; *Korenaga*, 2003]. It is therefore conceivable that the average water content of the upper mantle (100 ppm) is entirely due to the subduction of surface water taking into account the increasing recycling efficiency of subduction over time. This implies that the time-averaged subduction efficiency of H_2O is a factor of 3.9 less than our present-day estimate, or about 9%. This is in reasonable agreement with the low time-averaged subduction efficiency that is necessary to explain the heavy noble gas composition of the mantle [*Holland and Ballentine*, 2006].

[34] The increase in subduction efficiency implies that recently recycled material has significantly higher water content than the average upper mantle. This provides a natural explanation for the higher water concentrations in the plume source inferred by *Dixon et al.* [2002]. The geochemical record provides further suggestions for a change from dry to wet subduction [*McCulloch and Gamble*, 1991]. Recent geodynamic work [*Brandenburg et al.*, 2008] suggests that the mantle array between HIMU-EM1-DMM (high μ ($\mu = {}^{238}U/{}^{240}Pb$)-enriched mantle 1–depleted MORB mantle) in the U-Th-Pb, Sm-Nd, Rb-Sr, and Re-Os systems can be satisfactorily explained by oceanic crust recycling over the age of the Earth, provided that "wet" subduction did not start until 2.5 Ga. The EM1 component is associated with old oceanic crust, whereas HIMU is associated with young oceanic crust. This confirms an earlier qualitative suggestion by *Hart et al.* [1986]. If this view is correct, EM1 plumes should be significantly drier than HIMU plumes. While the EM plume source is generally considered to be drier than that of focus zone (FOZO) [e.g., *Dixon et al.*, 2002], it has proven difficult to determine the water concentration of the HIMU source.

4.3. Remaining Questions

[35] This study serves to highlight many new areas for future research.

[36] 1. The hydration state of the incoming slab is poorly known; speculation that significant hydration of the slab mantle happens in the trench outer rise should be tested by geophysical techniques, including seismology, gravity, and magnetism (since serpentinization produces magnetite). The hydration state of the oceanic lithosphere is expected to be heterogeneous, based on the presence of seamounts and ocean core complexes [e.g., *Blackman et al.*, 1998], and may vary dramatically from one subduction zone to another.

[37] 2. The role of unusual bulk compositions produced by metasomatism [*Bebout*, 2007] must be assessed. If phyllosilicate-rich rocks form along the contacts between different rocks (e.g., blackwall alteration rinds), these could be major H_2O carriers.

[38] 3. Fluid flow paths and the interaction between fluids and physical properties of the slab and wedge [e.g., *Cagnioncle et al.*, 2007; *Hebert et al.*, 2009] must be better understood. It is entirely possible that much of the H_2O that is considered to be expelled from the slab actually migrates to structurally deeper levels in the slab [*Hacker et al.*, 2003b; *Faccenda et al.*, 2009] and is subducted to much greater depth than expected. It is also likely that fluid flow paths are not vertical, such that the places where fluid actually leaves the slab may differ significantly from the places where the fluid was generated.

[39] 4. The role of "solid" diapirs in carrying fluid into the mantle wedge [*Gerya and Yuen*, 2003; *Behn et al.*, 2009] must be evaluated.

[40] 5. Better activity models are needed for phases such as melt, K-bearing clinopyroxene, and nominally anhydrous minerals.

[41] 6. The effects of volatiles other than H_2O (e.g., F can raise the temperature stability of mica and amphibole by 100–200°C) in stabilizing hydrous phases must be considered.

5. Conclusions

[42] We have provided a new estimate for the global dehydration of slabs in subduction zones using high-resolution thermal models and improved petrological modeling. The global flux estimates are somewhat lower than those of previous compilations but still allow for significant return flow of H_2O to the mantle below 230 km depth. Several uncertainties remain that are principally in the hydration

state of the lower crust and upper mantle of the slab. Nevertheless, we note good agreement on a global level between our new results and existing reports of the global H_2O flux out of arcs, the relative concentrations between the upper mantle and plume sources, and requirements from noble gas geochemistry.

[43] **Acknowledgments.** The research presented here has been partially funded by the National Science Foundation through grants EAR 0646757 and OCE 0841075 to P.v.K., and EAR-0545441 to B.R.H. The comments of an anonymous reviewer were greatly appreciated. We thank Julie Bryce and Alison Shaw for discussions and George Helffrich for inspiration.

References

Abers, G. A., P. E. van Keken, E. A. Kneller, A. Ferris, and J. C. Stachnik (2006), The thermal structure of subduction zones constrained by seismic imaging: Implications for slab dehydration and wedge flow, *Earth Planet. Sci. Lett.*, *241*, 387–397, doi:10.1016/j.epsl.2005.11.055.

Aizawa, Y., A. Barnhoorn, U. H. Faul, J. D. Fitz Gerald, I. Jackson, and I. Kovacs (2008), Seismic properties of Anita Bay Dunite: An exploratory study of the influence of water, *J. Petrol.*, *49*, 841–855, doi:10.1093/petrology/egn007.

Arcay, D., E. Tric, and M.-P. Doin (2007), Slab surface temperature in subduction zones: Influence of the interpolate decoupling depth and upper plate thinning processes, *Earth Planet. Sci. Lett.*, *255*, 324–338, doi:10.1016/j.epsl.2006.12.027.

Barnes, J. D., Z. D. Sharp, T. P. Fischer, D. R. Hilton, and M. J. Carr (2009), Chlorine isotope variations along the Central American volcanic front and back arc, *Geochem. Geophys. Geosyst.*, *10*, Q11S17, doi:10.1029/2009GC002587.

Bebout, G. E. (1995), The impact of subduction-zone metamorphism on mantle-ocean chemical cycling, *Chem. Geol.*, *126*, 191–218, doi:10.1016/0009-2541(95)00118-5.

Bebout, G. E. (2007), Metamorphic chemical geodynamics of subduction zones, *Earth Planet. Sci. Lett.*, *260*(3–4), 373–393, doi:10.1016/j.epsl.2007.05.050.

Behn, M. D., G. Hirth, P. B. Kelemen, and B. R. Hacker (2009), Implications of sediment diapirs on the H_2O flux into the mantle at arcs, *Eos. Trans. AGU*, *90*(52), Fall Meet. Suppl., Abstract T31D-01.

Billen, M. I., M. Gurnis, and M. Simons (2003), Multiscale dynamics of the Tonga-Kermadec subduction zone, *Geophys. J. Int.*, *153*, 359–388, doi:10.1046/j.1365-246X.2003.01915.x.

Blackman, D. K., J. R. Cann, B. Janssen, and D. K. Smith (1998), Origin of extensional core complexes: Evidence from the Mid-Atlantic Ridge at Atlantis fracture zone, *J. Geophys. Res.*, *103*, 21,315–21,333, doi:10.1029/98JB01756.

Brandenburg, J. P., E. H. Hauri, P. E. van Keken, and C. J. Ballentine (2008), A multiple-system study of the geochemical evolution of the mantle with force-balanced plates and thermochemical effects, *Earth Planet. Sci. Lett.*, *276*, 1–13, doi:10.1016/j.epsl.2008.08.027.

Cagnioncle, A.-M., E. M. Parmentier, and L. T. Elkins-Tanton (2007), Effect of solid flow above a subducting slab on water distribution and melting at convergent plate boundaries, *J. Geophys. Res.*, *112*, B09402, doi:10.1029/2007JB004934.

Clift, P., and P. Vannucchi (2004), Controls on tectonic accretion versus erosion in subduction zones: Implications for the origin and recycling of the continental crust, *Rev. Geophys.*, *42*, RG2001, doi:10.1029/2003RG000127.

Connolly, J. A. D. (2009), The geodynamic equation of state: What and how, *Geochem. Geophys. Geosyst.*, *10*, Q10014, doi:10.1029/2009GC002540.

Currie, C. A., and R. D. Hyndman (2006), The thermal structure of subduction zone back arcs, *J. Geophys. Res.*, *111*, B08404, doi:10.1029/2005JB004024.

Cuvelier, C., A. Segal, and A. A. van Steenhoven (1986), *Finite Element Models and the Navier-Stokes Equations*, D. Reidel, Dordrecht, Netherlands.

Dixon, J. E., L. Leist, C. Langmuir, and J.-G. Schilling (2002), Recycled dehydrated lithosphere observed in plume-influenced mid-oceanic-ridge basalt, *Nature*, *420*, 385–389, doi:10.1038/nature01215.

Faccenda, M., T. V. Gerya, and L. Burlini (2009), Deep slab hydration induced by bending-related variations in tectonic pressure, *Nat. Geosci.*, *2*, 790–793, doi:10.1038/ngeo656.

Furukawa, Y., and S. Uyeda (1989), Thermal state under the Tohoku arc with consideration of crustal heat generation, *Tectonophysics*, *164*, 175–187, doi:10.1016/0040-1951(89)90011-5.

Gerya, T. V., and D. A. Yuen (2003), Rayleigh-Taylor instabilities from hydration and melting propel "cold plumes" at subduction zones, *Earth Planet. Sci. Lett.*, *212*, 47–62, doi:10.1016/S0012-821X(03)00265-6.

Grove, T. L., N. Chatterjee, S. W. Parman, and E. Médard (2006), The influence of H_2O on mantle wedge melting, *Earth Planet. Sci. Lett.*, *249*, 74–89, doi:10.1016/j.epsl.2006.06.043.

Hacker, B. R. (2008), H_2O subduction beyond arcs, *Geochem. Geophys. Geosyst.*, *9*, Q03001, doi:10.1029/2007GC001707.

Hacker, B. R., and G. A. Abers (2004), Subduction factory: 3. An Excel Worksheet and macro for calculating the densities, seismic wave speeds, and H_2O contents of minerals and rocks at pressure and temperature, *Geochem. Geophys. Geosyst.*, *5*, Q01005, doi:10.1029/2003GC000614.

Hacker, B. R., G. A. Abers, and S. M. Peacock (2003a), Subduction factory: 1. Theoretical mineralogy, densities, seismic wave speeds, and H_2O contents, *J. Geophys. Res.*, *108*(B1), 2029, doi:10.1029/2001JB001127.

Hacker, B. R., S. M. Peacock, G. A. Abers, and S. D. Holloway (2003b), Subduction factory: 2. Are intermediate depth earthquakes in subducting slabs linked to metamorphic dehydration reactions?, *J. Geophys. Res.*, *108*(B1), 2030, doi:10.1029/2001JB001129.

Hart, S., D. C. Gerlach, and W. M. White (1986), A possible new Sr-Nd-Pb mantle array and consequences for mantle mixing, *Geochim. Cosmochim. Acta*, *50*, 1551–1557, doi:10.1016/0016-7037(86)90329-7.

Hashida, T. (1989), Three-dimensional seismic attenuation structure beneath the Japanese islands and its tectonic and thermal implications, *Tectonophysics*, *159*, 163–180, doi:10.1016/0040-1951(89)90126-1.

Hebert, L. B., P. Antoschechkina, P. Asimow, and M. Gurnis (2009), Emergence of a low-viscosity channel in subduction zones through the coupling of mantle flow and thermodynamics, *Earth Planet. Sci. Lett.*, *278*, 243–256, doi:10.1016/j.epsl.2008.12.013.

Hilton, D. R., T. P. Fischer, and B. Marty (2002), Noble gases and volatile recycling at subduction zones, in *Noble Gas Geochemistry and Cosmochemistry*, *Rev. Mineral. Geochem.*, vol. 47, edited by J. Matsuda, pp. 319–370, Mineral. Soc. of Am., Reston, Va., doi:10.2138/rmg.2002.47.9.

Hirschmann, M. M. (2006), Water, melting, and the deep Earth H_2O cycle, *Annu. Rev. Earth Planet. Sci.*, *34*, 629–653, doi:10.1146/annurev.earth.34.031405.125211.

Hirth, G., and D. L. Kohlstedt (1996), Water in the oceanic upper mantle: Implications for rheology, melt extraction and the evolution of the lithosphere, *Earth Planet. Sci. Lett.*, *144*, 93–108, doi:10.1016/0012-821X(96)00154-9.

Holland, G., and C. J. Ballentine (2006), Seawater subduction controls the heavy noble gas composition of the mantle, *Nature*, *441*, 186–191, doi:10.1038/nature04761.

Holland, T. J. B., and R. Powell (1998), An internally consistent thermodynamic data set for phases of petrological interest, *J. Metamorph. Geol.*, *16*, 309–343, doi:10.1111/j.1525-1314.1998.00140.x.

Hyndman, R. D., and S. M. Peacock (2003), Serpentinization of the forearc mantle, *Earth Planet. Sci. Lett.*, *212*, 417–432, doi:10.1016/S0012-821X(03)00263-2.

Ivandic, M., I. Grevemeyer, A. Berhorst, E. R. Flueh, and K. D. McIntosh (2008), Impact of bending related faulting on the seismic properties of the incoming oceanic plate offshore of Nicaragua, *J. Geophys. Res.*, *113*, B05410, doi:10.1029/2007JB005291.

Jadamec, M. A., and M. I. Billen (2010), Reconciling surface plate motions with rapid three-dimensional mantle flow around a slab edge, *Nature*, *465*, 338–341, doi:10.1038/nature09053.

Jarrard, R. D. (2003), Subduction fluxes of water, carbon dioxide, chlorine and potassium, *Geochem. Geophys. Geosyst.*, *4*(5), 8905, doi:10.1029/2002GC000392.

Jung, H., and S. Karato (2001), Water-induced fabric transitions in olivine, *Science*, *293*, 1460–1463, doi:10.1126/science.1062235.

Karato, S., and P. Wu (1993), Rheology of the upper mantle: A synthesis, *Science*, *260*, 771–778, doi:10.1126/science.260.5109.771.

Kelley, K. A., T. Plank, S. Newman, E. M. Stolper, T. L. Grove, S. Parman, and E. H. Hauri (2010), Mantle melting as a function of water content beneath the Mariana Arc, *J. Petrol.*, *51*, 1711–1738, doi:10.1093/petrology/egq036.

Kirby, S. H., W. B. Durham, and L. A. Stern (1991), Mantle phase changes and deep-earthquake faulting in subducted lithosphere, *Science*, *252*, 216–225, doi:10.1126/science.252.5003.216.

Kirby, S. H., E. R. Engdahl, and R. Denlinger (1996), Intermediate-depth intraslab earthquakes and arc volcanism as physical expressions of crustal and uppermost mantle metamorphism in subducting slabs, in *Subduction: Top to Bottom*, *Geophys. Monogr. Ser.*, vol. 96, edited by G. Bebout, pp. 195–214, AGU, Washington, D. C.

Kita, S., T. Okada, J. Nakajima, T. Matsuzawa, and A. Hasegawa (2006), Existence of a seismic belt in the upper plane of the double seismic zone extending in the along-arc direction at depths of 70–100 km beneath NE Japan, *Geophys. Res. Lett.*, *33*, L24310, doi:10.1029/2006GL028239.

Korenaga, J. (2003), Energetics of mantle convection and the fate of fossil heat, *Geophys. Res. Lett.*, *30*(8), 1437, doi:10.1029/2003GL016982.

Lee, C., and S. D. King (2009), Effect of mantle compressibility on the thermal and flow structures of subduction zones, *Geochem. Geophys. Geosyst.*, *10*, Q01006, doi:10.1029/2008GC002151.

Lee, C., and S. D. King (2010), Why are high-Mg# andesites widespread in the western Aleutians? A numerical model approach, *Geology*, *38*, 583–586, doi:10.1130/G30714.1.

Lefeldt, M., I. Grevemeyer, J. Gossler, and J. Bialas (2009), Intraplate seismicity and related mantle hydration at the Nicaraguan trench outer rise, *Geophys. J. Int.*, *178*, 742–752, doi:10.1111/j.1365-246X.2009.04167.x.

MacKenzie, L. M., G. A. Abers, S. Rondenay, and K. M. Fischer (2010), Imaging a steeply dipping subducting slab in southern Central America, *Earth Planet. Sci. Lett.*, *296*, 459–468, doi:10.1016/j.epsl.2010.05.033.

McCulloch, M. T., and J. A. Gamble (1991), Geochemical and geodynamical constraints on subduction zone magmatism, *Earth Planet. Sci. Lett.*, *102*, 358–374, doi:10.1016/0012-821X(91)90029-H.

Nadeau, S., P. Philippot, and F. Pineau (1993), Fluid inclusion and mineral isotopic compositions (H-C-O) in eclogitic rocks as tracers of loca fluid migration during high-pressure metamorphism, *Earth Planet. Sci. Lett.*, *114*, 431–448, doi:10.1016/0012-821X(93)90074-J.

Nakajima, J., Y. Tsuji, A. Hasegawa, S. Kita, T. Okada, and T. Matsuzawa (2009), Tomographic imaging of hydrated crust and mantle in the subducting Pacific slab beneath Hokkaido, Japan: Evidence for dehydration embrittlement as a cause of interslab earthquakes, *Gondwana Res.*, *16*, 470–481, doi:10.1016/j.gr.2008.12.010.

Peacock, S. M. (1990), Fluids processes in subduction zones, *Science*, *248*, 329–337, doi:10.1126/science.248.4953.329.

Peacock, S. M., and K. Wang (1999), Seismic consequences of warm versus cool subduction metamorphism: Examples from southwest and northeast Japan, *Science*, *286*, 937–939, doi:10.1126/science.286.5441.937.

Plank, T., and C. H. Langmuir (1998), The chemical composition of subducting sediment and its consequences for the crust and mantle, *Chem. Geol.*, *145*, 325–394, doi:10.1016/S0009-2541(97)00150-2.

Plank, T., L. B. Cooper, and C. E. Manning (2009), Emerging geothermometers for estimating slab surface temperatures, *Nat. Geosci.*, *2*, 611–615, doi:10.1038/ngeo614.

Ranero, C. R., J. P. Morgan, K. McIntosh, and C. Reichert (2003), Bending related faulting and mantle serpentinization at the Middle America Trench, *Nature*, *425*, 367–373, doi:10.1038/nature01961.

Rondenay, S., G. A. Abers, and P. E. van Keken (2008), Seismic imaging of subduction zone metamorphism, *Geology*, *36*, 275–278, doi:10.1130/G24112A.1.

Rüpke, L. H., J. P. Morgan, and J. A. D. Connolly (2004), Serpentine and the subduction zone water cycle, *Earth Planet. Sci. Lett.*, *223*, 17–34, doi:10.1016/j.epsl.2004.04.018.

Rychert, C., K. M. Fischer, G. A. Abers, T. Plank, E. Syracuse, J. M. Protti, V. Gonzalez, and W. Strauch (2008), Strong along-arc variation in attenuation in the mantle wedge beneath Costa Rica and Nicaragua, *Geochem. Geophys. Geosyst.*, *9*, Q10S10, doi:10.1029/2008GC002040.

Schmidt, M. W., and S. Poli (2003), Generation of mobile components during subduction of oceanic crust, in *Treatise on Geochemistry*, vol. 3, *The Crust*, edited by R. Rudnick, pp. 567–591, Elsevier, New York.

Schmidt, M. W., D. Vielzeuf, and E. Auzanneau (2004), Melting and dissolution of subducted crust at high pressures: The key role of white mica, *Earth Planet. Sci. Lett.*, *228*, 65–84, doi:10.1016/j.epsl.2004.09.020.

Scholl, D. W., and R. von Huene (2007), Crustal recycling at modern subduction zones applied to the past: Issues of growth and preservation of continental basement crust, mantle geochemistry, and supercontinent reconstruction, in *4D Framework of Continental Crust*, edited by R. D. Hatcher et al., *Mem. Geol. Soc. Am.*, 200, 9–33.

Shaw, A. M., E. H. Hauri, T. P. Fischer, D. R. Hilton, and K. A. Kelley (2008), Hydrogen isotopes in Mariana arc melt inclusions: Implications for subduction dehydration and the deep-Earth water cycle, *Earth Planet. Sci. Lett.*, *275*, 138–145, doi:10.1016/j.epsl.2008.08.015.

Skora, S., and J. Blundy (2010), High-pressure hydrous phase relations of radiolarian clay and implications for the involvement of subducted sediment in arc magmatism, *J. Petrol.*, *51*(11), 2211–2243, doi:10.1093/petrology/egq054.

Stachnik, J. C., G. A. Abers, and D. H. Christensen (2004), Seismic attenuation and mantle wedge temperatures in the Alaska subduction zone, *J. Geophys. Res.*, *109*, B10304, doi:10.1029/2004JB003018.

Stein, C. A., and S. Stein (1992), A model for the global variation in oceanic depth and heat-flow with lithospheric age, *Nature*, *359*, 123–129, doi:10.1038/359123a0.

Syracuse, E. M., and G. A. Abers (2006), Global compilation of variations in slab depth beneath arc volcanoes and implications, *Geochem. Geophys. Geosyst.*, *7*, Q05017, doi:10.1029/2005GC001045.

Syracuse, E. M., G. A. Abers, K. Fischer, L. MacKenzie, C. Rychert, M. Protti, V. Gonzalez, and W. Strauch (2008), Seismic tomography and earthquake locations in the Nicaraguan and Costa Rican upper mantle, *Geochem. Geophys. Geosyst.*, *9*, Q07S08, doi:10.1029/2008GC001963.

Syracuse, E. M., P. E. van Keken, and G. A. Abers (2010), The global range of subduction zone thermal models, *Phys. Earth Planet. Inter.*, *51*(8), 1761–1782, doi:10.1016/j.pepi.2010.02.004.

Tollstrup, D., J. Gill, A. Kent, D. Prinkey, R. Williams, Y. Tamura, and O. Ishizuka (2010), Across-arc geochemical trends in the Izu-Bonin arc: Contributions from the subducting slab, revisited, *Geochem. Geophys. Geosyst.*, *11*, Q01X10, doi:10.1029/2009GC002847.

van Keken, P. E., B. Kiefer, and S. M. Peacock (2002), High-resolution models of subduction zones: Implications for mineral dehydration reactions and the transport of water to the deep mantle, *Geochem. Geophys. Geosyst.*, *3*(10), 1056, doi:10.1029/2001GC000256.

van Keken, P. E., C. Currie, S. D. King, M. D. Behn, A. Cagnioncle, J. He, R. F. Katz, S.-C. Lin, M. Spiegelman, and K. Wang (2008), A community benchmark for subduction zone modeling, *Phys. Earth Planet. Inter.*, *171*, 187–197, doi:10.1016/j.pepi.2008.04.015.

Vlaar, N. J., P. E. van Keken, and A. P. van den Berg (1994), Cooling of the Earth in the Archaean, *Earth Planet. Sci. Lett.*, *121*, 1–18, doi:10.1016/0012-821X(94)90028-0.

Wada, I., and K. L. Wang (2009), Common depth of slab-mantle decoupling: Reconciling diversity and uniformity of subduction zones, *Geochem. Geophys. Geosyst.*, *10*, Q10009, doi:10.1029/2009GC002570.

Wallace, P. J. (2005), Volatiles in subduction zone magmas: concentrations and fluxes based on melt inclusion and volcanic gas data, *J. Volcanol. Geotherm. Res.*, *140*, 217–240, doi:10.1016/j.jvolgeores.2004.07.023.

Wiens, D. A., K. A. Kelley, and T. Plank (2006), Mantle temperature variations beneath back-arc spreading centers inferred from seismology, petrology and bathymetry, *Earth Planet. Sci. Lett.*, *248*, 16–27, doi:10.1016/j.epsl.2006.04.011.

Yoshimoto, K., U. Wegler, and A. Korn (2006), A volcanic front as a boundary of seismic attenuation structures in northeastern Honshu, Japan, *Bull. Seismol. Soc. Am.*, *96*, 637–646, doi:10.1785/0120050085.

G. A. Abers, Lamont-Doherty Earth Observatory, Columbia University, PO Box 1000, 61 Rt. 9W, Palisades, NY 10964, USA. (abers@ldeo.columbia.edu)

B. R. Hacker, Department of Earth Science, University of California, Santa Barbara, CA 93109-9630, USA. (hacker@geol.ucsb.edu)

E. M. Syracuse, Department of Geoscience, University of Wisconsin–Madison, 1215 W. Dayton St., Madison, WI 53706, USA. (syracuse@geology.wisc.edu)

P. E. van Keken, Department of Geological Sciences, University of Michigan, Ann Arbor, MI 48105, USA. (keken@umich.edu)